Analysis of Squirrel Cage Induction Machine Based on the Magductance Modulator

Zhengzhou Ma, *Student Member, IEEE*, Ming Cheng, *Fellow, IEEE*, Wei Qin, *Member, IEEE*, Peng Han, Zheng Wang, and Wei Hua, *Senior Member, IEEE*

***Abstract*—In order to conduct an explicit analysis of the induction machine (IM), the sole magnetic field parameter's description of short-circuited coils (SCC) modulator is crucial, despite its absence in the literature. This article presents a novel concept of introducing magductance into the SCC, thus referring to the SCC modulator as the magductance modulator. The modulation operator is completely studied from magnetic field parameters, thereby adding in understanding the working principle of IM. Expressions for the modulated magnetomotive force (MMF) is elucidated specifically for the squirrel cage induction machine (SCIM). Unique vector modulation to the magductance modulator is unveiled. Then, the effects of modulator parameters on machine performance are investigated. The calculation process based on the proposed method is illustrated in detail, with the key performance parameter expressed. The proposed method is validated through comparisons with finite element analysis (FEA) and experimental results.**

***Index Terms*—Induction machine (IM), magductance, magnetic field modulation theory, vector modulation.**

I. Introduction

INDUCTION machine (IM) with squirrel cage has been a hot spot over the last decades due to the fact that it is the most conventional ac electrical machine and offers significant advantages over other counterparts, including reliability, mature, manufacture convenience, and simple operation. The major methods to analyze IM can be classified into two categories. The first method adopting the equivalent electrical circuit is mostly applied [1], [2], [3], while it cannot investigate the effect of structural parameters on magnetic field directly. The second method combines the first one with winding function [4], [5], [6], and the effect of rotor topology on performance is researched initially. Besides, the lack of expressions for magnetic field exists in both methods, making them hard to compare between different harmonics components directly.

The general airgap field modulation theory (GAFMT) for electrical machines is a unified approach for modeling the torque production and operation principle of different types of electrical machines [7], [8], in which the contributions of magnetic field harmonics to machine performance are available in mathematical expression perspective. Thus, the GAFMT provides a new perspective for principle understanding and performance analysis for different types of electrical machines. In the GAFMT, there are three types of modulators, namely salient pole reluctance (SPR), flux barriers (FBS), and short-circuited coils (SCC). In analyzing the SPR and FBS modulators, their modulation effects are clearly revealed by using the magnetic parameter of permeance [9], [10]. Through investigating the conversion factors, the modulator parameters, including the slotting depth and pole arc coefficient, are analyzed and optimized [11]. Since there lacks a magnetic parameter describing the modulation behavior of SCC modulator, however, the modulated magnetomotive force (MMF) was calculated indirectly by multiplying the winding function with the induced current in the SCC modulator [12]. The knowledge of SCC modulator mostly relies on finite element analysis (FEA) [13], [14], [15] by now. As a consequence, the IM's working principle may still not be understood from the view of magnetic field parameters explicitly.

Recently, a novel parameter for magnetism, named as magductance (or magnetic inductance), has been proposed to characterize the closed conductive coil [16]. The traditional scalar magnetic circuit theory with sole component of reluctance is promoted to the vector one featured by reluctance and magductance, and the transformer is completely analyzed from magnetic field parameters. Considering the similar working principles of transformer and IM, it is reasonable to introduce the magductance into the IM analysis. With the aid of magductance, it is expected to clarify the modulation effect of SCC modulator similar to that of SPR and FBS modulators.

Derived from above, this article aims to analyze the squirrel cage induction machine (SCIM) by virtue of magductance. The concept of magductance modulator is introduced into the SCC modulator first, with its modulation operator studied completely from magnetic field parameters. The modulated MMF then is expressed. Unique vector modulation (reflected by magnetic field conversion factor C_{vp} and phase shift φ) is revealed and further analyzed. It is worth noting that the phase shift φ between source MMF and modulated MMF is capable of being

Manuscript received 7 October 2023; revised 4 January 2024 and 7 March 2024; accepted 11 April 2024. Date of publication 17 May 2024; date of current version 11 October 2024. This work was supported by the National Natural Science Foundation of China under Projects 51991381 and 52250065. *(Corresponding author: Ming Cheng.)*

Zhengzhou Ma, Ming Cheng, Wei Qin, Zheng Wang, and Wei Hua are with the School of Electrical Engineering, Southeast University, Nanjing 210096, China (e-mail: mzz_ee@seu.edu.cn; mcheng@seu.edu.cn; qinwei986@seu.edu.cn; zwang@seu.edu.cn; huawei1978@seu.edu.cn).

Peng Han is with the Ansys Inc., San Jose, CA 95134 USA (e-mail: peng.han@ansys.com).

Color versions of one or more figures in this article are available at https://doi.org/10.1109/TIE.2024.3392998.

Digital Object Identifier 10.1109/TIE.2024.3392998

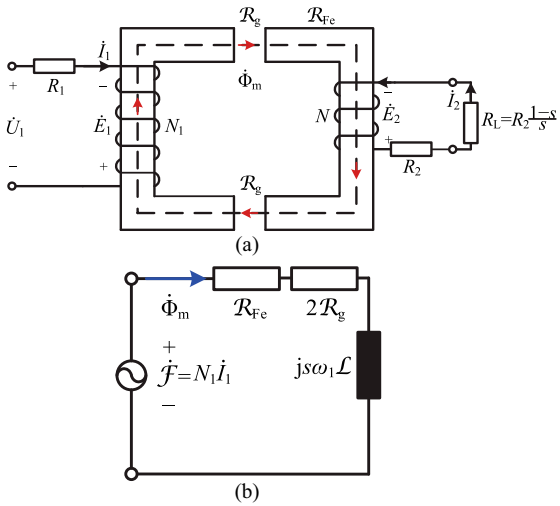

Fig. 1. Equivalent the SCIM. (a) Electromagnetic structure. (b) Equivalent vector magnetic circuit.

investigated intuitively through the proposed method. Effects of modulator parameters on machine performance are investigated consequently. Merits of the proposed method are summarized by comparing with original GAFMT. The calculation process of proposed method is illustrated in detail, and the calculated results are verified by comparing with FEA results and experimental ones. The calculated results prove the feasibility of proposed method. More importantly, it makes another trial of understanding the working principle of SCIM from a new perspective, and the analysis of SCC modulator may be illustrated as similar as that of SPR modulator and FBS one.

II. Magductance Modulator's Working Principle

A. Concept of Magductance Modulator

According to [16], a closed conductive coil can be characterized as magductance (or magnetic-inductance). The magductance represents the effect of a closed conductor coil on hindering the variation of magnetic flux which flows through the coil, and it is expressed as

$$\mathcal{L} = N^2/R \tag{1}$$

where $\mathcal{L}$ is the magductance of the closed conductive coil. N is the number of turns in the closed conductive coil. R is the resistance of closed conductive coil.

The electromagnetic structure of SCIM is shown in Fig. 1(a), where U_1 is the input voltage of stator winding, R_1 the stator winding resistance, N_1 the stator winding's number of turns, E_1 the induced electromotive force (EMF) of stator winding, I_1 the stator winding current, Φ_m the amplitude of magnetic flux, $\mathcal{R}_g$ the airgap reluctance, $\mathcal{R}_{Fe}$ the iron core reluctance, E_2 the SCC induced EMF, I_2 the SCC current, R_L the equivalent load resistance of mechanical output power, and s the slip frequency.

The working principle of SCIM is similar to that of transformer analyzed in [16]. Differences lie in:

1) In addition to the iron core reluctance, there adds $\mathcal{R}_g$ corresponding to the airgap in the SCIM.
2) The squirrel cage winding located at the rotor is equivalent to be the magductance.

The equivalent vector magnetic circuit introducing the magductance is shown in Fig. 1(b), where ω_1 is the electrical angular velocity of stator winding. Because the rotor rotates at slip speed relative to the magnetic field established by stator winding, the current frequency in the squirrel cage winding is slip frequency $s\omega_1$.

The MMF balance equation in the SCIM then can be expressed as

$$\begin{aligned}\dot{\mathcal{F}} &= 2\mathcal{R}_g\dot{\Phi}_m + \mathcal{R}_{Fe}\dot{\Phi}_m + js\omega_1\mathcal{L}\dot{\Phi}_m \\ &= \mathcal{R}\dot{\Phi}_m + js\omega_1\mathcal{L}\dot{\Phi}_m\end{aligned} \tag{2}$$

where $\mathcal{R} = 2\mathcal{R}_g + \mathcal{R}_{Fe}$.

From (2), the previous SCC modulator can also be referred to as the magductance modulator, as it modulates the amplitude and phase of source MMF established by stator winding.

B. Modulation Operator

The modulation behavior of magductance modulator can be characterized by introducing the modulation operator. For the sake of simplicity, some assumptions are made as follows.

1) The airgap of SCIM is uniform whilst no rotor eccentricity exists, with Carter's factor denoting the stator slotting effect.
2) The conductors in each stator slot is located at the middle point of slot opening.
3) The end effect from rotor end rings is considered through calculating the equivalent magductance, and the flux leakage from both sides of SCIM is not considered.

According to the linearity law of modulator [7], decompose modulators in the SCIM, and the modulated MMF consists of two parts. The first one is the MMF established by the rotor SPR modulator. The second one corresponds to the MMF established by the magductance modulator. The joint action of SPR modulator and magductance modulator modulates the amplitude and phase of source MMF.

The improved modulation operator by introducing the magductance modulator is expressed as

$$\begin{aligned}&M(\mathcal{L})[f(\phi,t)] \\ &= \begin{cases}\left[f(\phi,t) - \mathcal{L}(\phi)\lambda_{RT}(\phi)\dfrac{df(\phi,t)}{dt}\right] \Big/ \sqrt{1+(L_2\lambda)^2}, \phi \in C^S \\ f(\phi,t), \phi \in [0,2\pi] - C^S\end{cases}\end{aligned} \tag{3}$$

where $f(\phi, t)$ is the MMF established by stator windings. $\mathcal{L}(\phi)$ is the spatial distribution function of magductance modulator. $\lambda_{RT}(\phi)$ is the permeance function of rotor SPR modulator [17]. $\mathcal{L}_2$ and λ are respectively the magnitude of $\mathcal{L}(\phi)$ and $\lambda_{RT}(\phi)$. C^S is the mechanical radians occupied by magductance modulator.

Different from the original GAFMT where only the amplitude modulation was considered, the magductance modulator also modulates the phase as denoted by $\mathcal{L}(\phi)\lambda_{RT}(\phi)df(\phi, t)/dt$. If $\mathcal{L}(\phi) = 0$, i.e., no magductance modulator exists, the MMF is solely established by stator windings, thus $M(\mathcal{L})[f(\phi, t)] = f(\phi, t)$. If the magductance modulator works, i.e., $\mathcal{L}(\phi) \neq 0$, it will

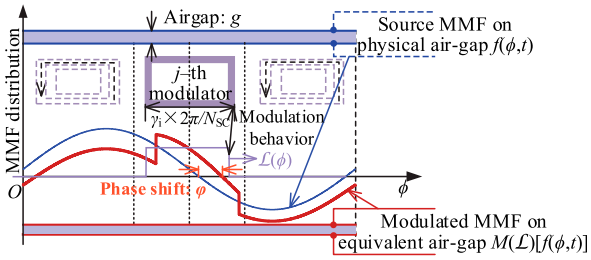

Fig. 2. The modulation operator of magductance modulator.

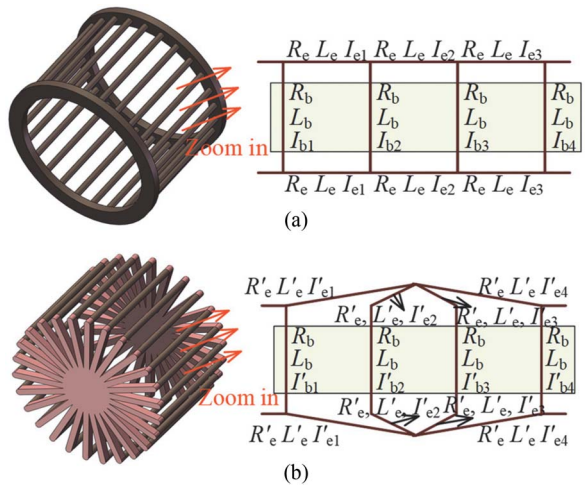

Fig. 3. Topology and parameters of the squirrel cage rotor. (a) Original cage rotor. (b) Equivalent cage rotor.

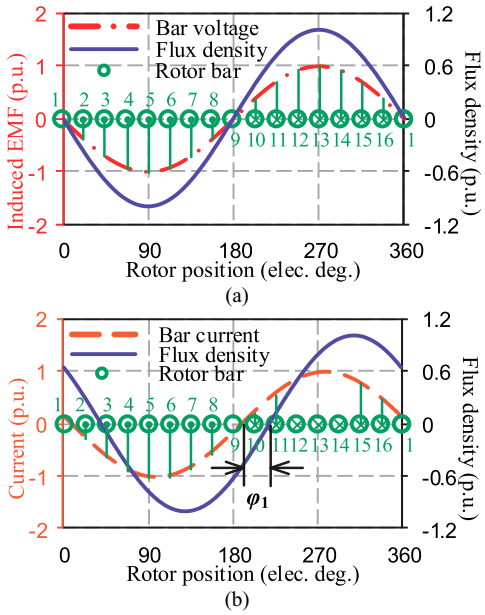

Fig. 4. Distribution of induced EMF and current in each bar of the squirrel cage rotor. (a) Induced EMF. (b) Current.

modulate the amplitude and phase of MMF shown in Fig. 2. This is why the previous SCC modulator is renamed as the magductance modulator. From this point of view, introducing the magductance enriches the original GAFMT from the scalar modulation in amplitude to the vector one in both amplitude and phase. Given that $\lambda_{RT}(\phi)$ and $f(\phi, t)$ are available, the expression for $\mathcal{L}(\phi)$ of squirrel cage is the key to calculating machine performance and is illustrated next.

C. Calculation of Equivalent Magductance

Topology and parameters of the squirrel cage rotor are illustrated in Fig. 3, where R_b, L_b, and I_b are respectively the original resistance, inductance, and current of rotor bar, R_e, L_e, and I_e are respectively the original resistance, inductance, and current of common end ring, R'_e, L'_e, and I'_e are respectively the equivalent resistance, inductance, and current of common end ring. Derived from above, identical current flows through rotor bars that make up one magductance element. However, for the squirrel cage rotor as shown in Fig. 3(a), the current in the common end ring is not equal to that in the attached rotor bars, i.e., $I_{bm} \neq I_{em}$, where $m = 1, 2, 3, \ldots, N_{SC}$. N_{SC} is the number of rotor bars per pole-pair. At this time, on the one hand, the resistance of rotor bar and rotor end ring cannot be added directly for the sake of non-identical current. On the other hand, the end effects from rotor end rings cannot be ignored because they also affect SCIM performance [18], [19], [20], [21], [22]. The equivalent electrical circuit method normally determines parameters through experimental tests [18] to consider end effects. With an advance in FEA, the parameters can also be determined from 2-D/3-D FEA [18], [19], [20]. In the winding function method, it takes into account the end effects by virtue of calculating the rotor end ring impedances in analytical formulas or FEA results [21], [22]. To calculate the SCIM performance accurately according to the magductance modulator, the equivalent magductance should consider the common end ring as shown in Fig. 3(b), at this time there satisfies $I'_{bm} = I'_{em}$, and the resistance of rotor bar and rotor end ring then can be summed up directly.

The distribution of induced EMF, current on the rotor bar, and magnetic flux density B_m established by stator windings is shown in Fig. 4, where φ_1 is the spatial phase difference between the current and B_m. Because of the relative motion between B_m and rotor, the induced EMFs in adjacent rotor bars have a phase shift

$$\alpha = 2\pi p / N_{SC} \tag{4}$$

where p is the pole pair numbers (PPN) of stator windings.

Because the structure of cage rotor is symmetrical, currents flowing through adjacent rotor bars also differ by α electrical angle, consequently the current flowing through the common end ring is the difference of adjacent rotor bar currents. To ensure that the output power is constant before and after modification, the polygon impedance of common end ring is transformed into star impedance as shown in Fig. 3(b)

$$\begin{cases} R'_e = \dfrac{R_e}{4[\sin(p\pi/N_{SC})])^2}, \\ L'_e = \dfrac{L_e}{4[\sin(p\pi/N_{SC})])^2}. \end{cases} \tag{5}$$

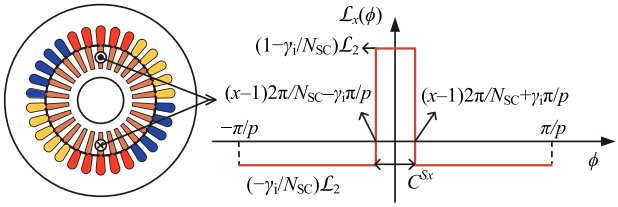

Fig. 5. Spatial distribution function of xth magductance modulator.

At this time there is $I'_{bm} = I'_{em}$, and the equivalent resistance R_2 and equivalent inductance L_2 of each rotor bar are

$$\begin{cases} R_2 = R_b + 2R'_e \\ L_2 = L_b + 2L'_e \end{cases}. \tag{6}$$

As two equivalent rotor bars make up one magductance element, the value of single magductance element $\mathcal{L}_2$ is

$$\mathcal{L}_2 = \frac{N_2^2}{2 \times (R_2 + \mathrm{j}s\omega_1 L_2)} \tag{7}$$

where N_2 is the number of turns of the squirrel cage.

As the value of resistance R_2 is much larger than that of leakage inductive reactance $s\omega_1 L_2$, R_2 is considered here, and the denominator of (7) is reexpressed as $2 \times R_2$. It is in accordance with the original expression in (1). The spatial distribution of xth magductance modulator is shown in Fig. 5, where γ_i is the span of single magductance modulator, C^{Sx} is the electrical radian of the xth magductance modulator, which is expressed by

$$C^{Sx} = [(x-1)2\pi/N_{SC} - \gamma_i\pi/p, (x-1)2\pi/N_{SC} + \gamma_i\pi/p] \tag{8}$$

where $x = 1, 2, 3, \ldots, N_{SC}$.

The distribution of magductance modulator $\mathcal{L}(\phi)$ is the superposition of magductance modulators corresponding to one pole–pair and is expressed as

$$\mathcal{L}(\phi) = \sum_{x=1}^{N_{SC}} \mathcal{L}_x(\phi) = \sum_{k=0}^{\infty} \frac{2N_{SC}\gamma_i\mathcal{L}_2}{m_1 k_w^2} \frac{\sin(k\gamma_i\pi)}{k\gamma_i\pi} \cos(kN_{SC}\phi). \tag{9}$$

From (9), it is available that by introducing the magductance modulator, its expression is similar to that of SPR modulator and FBS modulator. In addition, the magductance modulator is closely linked with its material and structural parameters, i.e., N_{SC}, γ_i, and $\mathcal{L}_2$. In terms of $\mathcal{L}_2$ there is

$$R_b = \frac{\rho l_{stk}}{S_{bar}} \tag{10}$$

where ρ is the resistivity. l_{stk} is the stacking length. S_{bar} is the cross-sectional area of single rotor bar. R_e is proportional to the end length between adjacent two rotor bars.

The spatial distribution of magductance modulator $\mathcal{L}(\phi)$ is illustrated in Fig. 6, taking a few N_{SC} (6, 12, 18, 22, and 26) as cases, whose detailed descriptions will be available in 1), Part A, Section III. It is noted that the variations of structural parameters are considered here. On the one hand, from Fig. 6, the peak value of magductance and its sinusoidal degree increases with N_{SC}, preliminarily proving that a sufficient value of N_{SC} facilitates improving the SCIM performance which works in single harmonic component. On the other hand, it also reflects that, with the aid of magductance, the analysis of SCC modulator in the SCIM may be conducted as similar as that of SPR modulator and FBS modulator. As under this situation, the structural variation of SCC modulator is contained in the $\mathcal{L}(\phi)$.

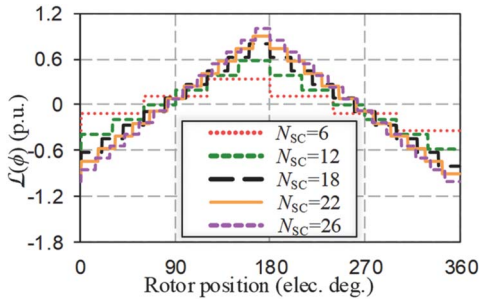

Fig. 6. Spatial distribution of magductance modulator.

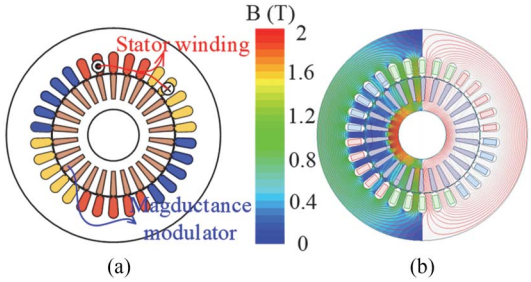

Fig. 7. Structure and field distribution of SCIM. (a) Machine cross-section. (b) No–load flux lines/density distribution.

TABLE I
MAJOR PARAMETERS OF SCIM

Symbol	Quantity	Value
N_{slot}	Number of stator slots	30
N_{SC}	Number of rotor bars	26
γ_i	Span of magductance modulator	0.5
p	PPN of stator windings	1
s	Slip frequency	0.03
N_{ph}	Number of turns per phase	185
R_{s_out}	Outer stator radius	105 mm
R_{s_in}	Inner stator radius	58 mm
R_{r_out}	Outer rotor radius	57.5 mm
R_{r_in}	Inner rotor radius	24 mm
g	Airgap length	0.5 mm
l_{stk}	Stacking length	125 mm
ω_1	Synchronous angular velocity	314 rad/s

D. Derivation of Modulated MMF in the SCIM

Derived from above, the modulated MMF can be expressed. The SCIM investigated in the article is shown in Fig. 7, and machine parameters are illustrated in Table I. For simplicity, the modulation effect of rotor SPR modulator is seen as unit modulation. Among the source MMF established by the stator windings, the primary p pole–pair harmonic component is solely

considered. They are respectively expressed as

$$\lambda_{\mathrm{RT}}(\phi) = \frac{\mu_0}{g} \tag{11}$$

where μ_0 is the vacuum permeability. g is the airgap length.

$$f(\phi, t) = F_1 \sin(p\phi - s\omega_1 t) \tag{12}$$

where

$$F_1 = \frac{m_1 N_{\mathrm{ph}} k_{\mathrm{w}} I_{\mathrm{m}}}{\pi p} \tag{13}$$

where m_1 is the number of phases of stator windings. k_{w} is the fundamental winding factor of stator windings. I_{m} is the current amplitude of stator windings.

Combining (3), (9), (11) with (12), the modulated MMF is

$$\begin{aligned} M(\mathcal{L})[f(\phi,t)] = {} & (F_1 - C_{\mathrm{vp}})\sin(p\phi - s\omega_1 t - \varphi) \\ & + \sum_{l=1}^{\infty} C_{\mathrm{sum}} \cos[(lN_{\mathrm{SC}} - p)\phi + s\omega_1 t] \\ & + \sum_{l=1}^{\infty} C_{\mathrm{dif}} \cos[(lN_{\mathrm{SC}} + p)\phi - s\omega_1 t] \end{aligned} \tag{14}$$

where C_{vp}, C_{sum}, and C_{dif} are magnetic field conversion factors, reflecting the modulation effect of magductance modulator.

Due to the modulation effect of magductance modulator, in addition to the p pole–pair harmonic component, other harmonic components are also generated whose values are reflected by C_{sum} and C_{dif}. Because the SCIM performance is mostly contributed by p pole–pair harmonic component, it is investigated here. For p pole–pair harmonic component, there emerges a phase shift φ, which reflects the phase difference between modulated MMF and source MMF. The modulated MMF is modulated by the SPR modulator and magductance modulator jointly, and it is reflected by $F_1 - C_{\mathrm{vp}}$ in (14). The magnetic field conversion factor C_{vp} and phase shift φ are respectively expressed as

$$C_{\mathrm{vp}} = \frac{F_1 2s\omega_1 \mathcal{L}_2 N_{\mathrm{SC}} \sin(\gamma_{\mathrm{i}} l\pi)\mu_0 r_{\mathrm{g}} l_{\mathrm{stk}} / \pi g p^2 l \gamma_{\mathrm{i}}}{\sqrt{1^2 + [2s\omega_1 \mathcal{L}_2 N_{\mathrm{SC}} \sin(\gamma_{\mathrm{i}} l\pi)\mu_0 r_{\mathrm{g}} l_{\mathrm{stk}} / \pi g p^2 l \gamma_{\mathrm{i}}]^2}} \tag{15}$$

$$\varphi = \arctan(2s\omega_1 \mathcal{L}_2 N_{\mathrm{SC}} \sin(\gamma_{\mathrm{i}} l\pi)\mu_0 r_{\mathrm{g}} l_{\mathrm{stk}} / \pi g p^2 l \gamma_{\mathrm{i}}). \tag{16}$$

From (15), when applying the magductance modulator, the amplitude of p pole–pair harmonic component in the modulated MMF is linked with the value of magductance. Likewise, the phase shift φ is also linked with the magductance from (16). When the rotor velocity varies from its synchronous angular velocity 314 rad/s to 0 rad/s, φ theoretically will vary from 0 and finally close to 90°. If the magductance modulator doesn't work, there satisfies $C_{\mathrm{vp}} = 0$ and $\varphi = 0$, and at this time, the modulated MMF is equal to the source MMF. To conclude, it is the effect of magductance modulator on source MMF that modulates the modulated MMF both in amplitude and phase.

III. Impact of the Magductance Modulator

As aforementioned, the magductance modulator shows unique characteristics in modulating both amplitude and phase. The impact of modulator on machine performance is investigated here, focusing on analyzing the relationship between machine performance and structural parameters. The average torque is selected as the target performance.

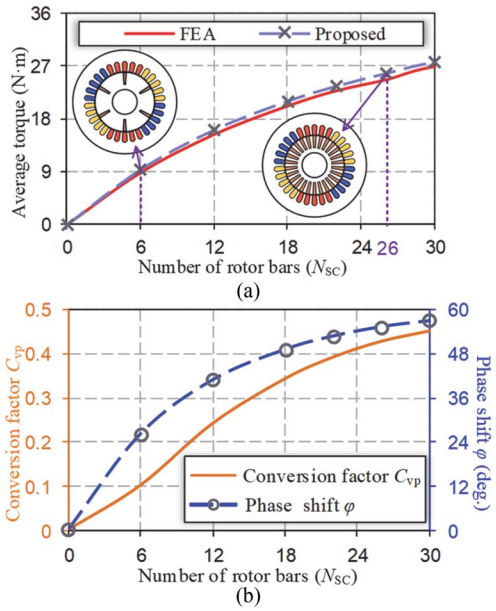

Fig. 8. Effect of N_{SC} on machine performance. (a) Average torque. (b) Magnetic field conversion factor C_{vp} and phase shift φ.

A. Parameters Effects

1) Number of Rotor Bars: The number of rotor bars N_{SC} is linked with the modulation effect as can be seen from (15) and (16). The comparisons of calculated average torque between 2-D FEA and the proposed method are shown in Fig. 8(a), where the number of rotor bars varies and the cross-sectional area of single rotor bar is fixed. It is noted that 2-D FEA is applied in this section, and the differences in the end effect between 2-D and 3-D FEA will be discussed later. The selected two machine topologies are shown in Fig. 8(a) where the N_{SC} is 6 and 26. It's also noted that effects of common end ring are considered here.

Calculated torque results from the proposed method coincide well with those from FEA. From Fig. 8(b), both of the magnetic field conversion factor C_{vp} and phase shift φ are proportional to N_{SC}. As illustrated in Table II, the value of magductance increases with N_{SC}, thus improves the modulation effect which is reflected by C_{vp} and φ.

2) Material Usage: To investigate the effects of material, in the magductance modulator, the material of aluminum and copper is compared here, with their conductivities respectively being 23 000 000 and 58 000 000 S/m. Effects of material on common end rings are also considered. The comparisons are concluded in Table III.

The torque when adopting copper is larger than that adopting aluminum, and results from the proposed method coincide well with FEA results. Meanwhile the phase shift φ adopting copper is larger than that adopting aluminum, as it is proportional to the value of magductance. Although copper is proven to be superior

TABLE II
CALCULATED VALUE OF MAGDUCTANCE

N_{SC}	$\mathcal{L}_2$ (Ω^{-1})	The Value of $\mathcal{L}(\phi)$ (Ω^{-1})	h_r (mm)	$\mathcal{L}_2$ (Ω^{-1})	The Value of $\mathcal{L}(\phi)$ (Ω^{-1})
0	0	0	0	0	0
6	2731.67	8195	6	818.69	10642.92
12	2445.43	14672.56	10	1176.84	15298.87
18	2202.45	19822.1	14	1478.41	19219.35
22	2064.52	22709.7	18	1735.83	22565.8
26	1975.63	25683.26	22	1975.63	25683.26
30	1833.91	27508.65	28	2239.71	29116.22

TABLE III
COMPARISON OF DIFFERENT MATERIAL

Compared Material		Aluminum	Copper
Magductance by the proposed method (Ω^{-1})		1975.63	4982.07
φ by the proposed method (°)		55.58	74.76
Torques (N·m)	Proposed method	25.9	52.76
	FEA	24.96	50.58
	Error (%)	3.77	4.3

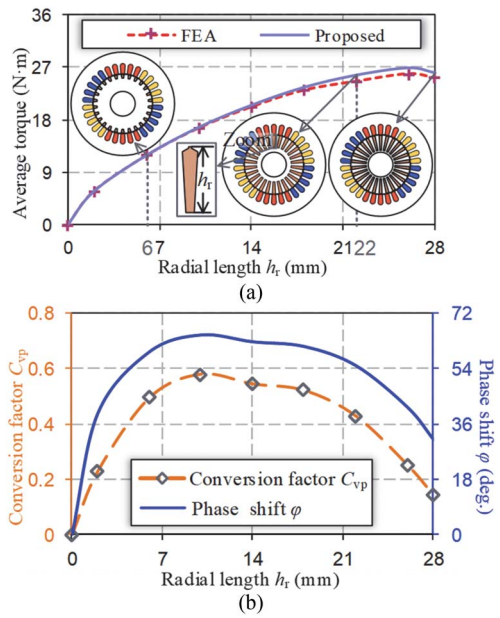

Fig. 9. Effect of radial length h_r on machine performance. (a) Average torque. (b) Conversion factor C_{vp} and phase shift φ.

to improving machine performance, aluminum is mostly applied for the sake of manufacture cost.

3) Radial Length: The effects of magductance modulator's radial length h_r on machine performance are investigated. A comparison is conducted between the average torque results and radial length as illustrated in Fig. 9(a), where three machine topologies with h_r being 6, 22, and 28 mm are shown.

The calculated torques from proposed method coincide well with FEA results. Besides, from Fig. 9(b), when h_r increases from 0 mm, the modulation effect of magductance modulator reflected by C_{vp} improves first and decreases later. The phase shift φ is also affected by the modulation effect, thus showing similar variation laws.

TABLE IV
SUMMARIES AND COMPARISONS OF THE TWO METHODS

Methods	Original GAFMT	Magductance Modulator–based
Calculation process	Indirect	Explicit
Performance calculation	√	√
Amplitude modulation	√	√
Phase modulation	×	√
Parameters analysis	×	√

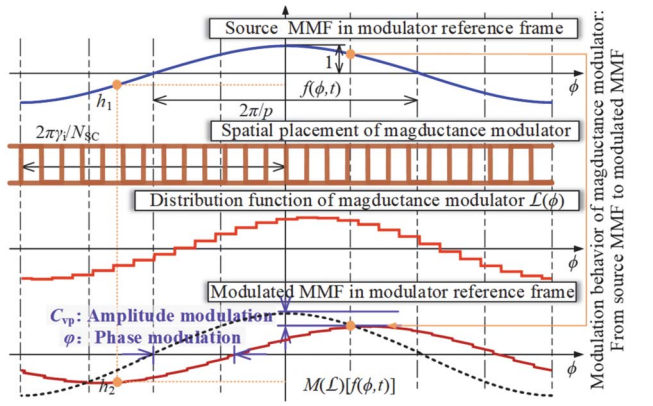

Fig. 10. Modulation behavior of magductance modulator.

B. Unique Characteristics of Magductance Modulator

Table IV summarizes the characteristics of proposed method based on the magductance modulator and that of original GAFMT, with their comparisons concluded as:

1) The proposed method calculates SCIM performance directly, whereas the original GAFMT calculated indirectly by the multiple of winding function and induced current.
2) The unique phase modulation to SCC is revealed by the magductance modulator. The magnetic field conversion factor C_{vp} and phase shift φ for p pole–pair are available from (15) and (16). Simultaneous considerations of amplitude and phase modulation are essential for an accurate analysis of modulation effect. By contrast, the phase modulation was not revealed effectively in the original GAFMT to some extent, as it was covered in the calculation process for modulated MMF.
3) With an introduction of magductance modulator, the analysis of modulator's parameters on modulation effect, including the number of rotor bars, material usage, and radial length, can be conducted accordingly. It's similar to that in the analysis of SPR and FBS modulator's parameters. In the original GAFMT, as the effect of SCC modulator on machine performance was investigated indirectly, the relationship between modulator parameters and modulation effect may not be available consequently.

The modulation behavior of magductance modulator is shown in Fig. 10, in the case of SCIM analyzed in this article. When the source MMF passes from the airgap to the magductance modulator, it multiples the synergetic effect of SPR modulator and magductance modulator to obtain the modulated MMF.

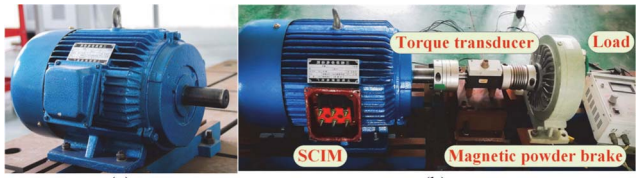

Fig. 11. Prototype and test rig of the SCIM. (a) Prototype. (b) Test rig.

Different from the SPR modulator [9], [23] and FBS modulator [24], [25] where both of them just modulate the amplitude of source MMF, the magductance modulator also modulates the phase, achieving the vector modulation effect as illustrated in the last row of Fig. 10.

To conclude, by introducing the magductance modulator, the contributions of proposed method lie in that: 1) It allows for a chance of analyzing the SCIM performance intuitively in magnetic parameters, i.e. reluctance and newly proposed magductance. 2) The relationships between the modulator parameters and machine performance are established directly, where the effects of the former on latter are reflected by unique vector modulation effect, i.e., C_{vp} in (15) and φ in (16). 3) The SCIM performance can be calculated conveniently whilst maintaining the calculation accuracy.

IV. Case Illustration

Section III has proven the unique modulation characteristics of magductance modulator. In order to verify the investigation above and the feasibility of proposed method, in this section, the specific case is illustrated in detail. The comparisons are conducted between calculated results, FEA results, and experimental ones. Because the SCIM is mostly applied for the motor mode, the output torque is selected as the machine parameter to be compared.

The experimental study was conducted on a standard Y2 series SCIM. The machine is supplied by the voltage source from power grid, in accordance with simulation condition in FEA as well as calculated condition from the proposed method. The prototype and test rig are shown in Fig. 11. Specific machine parameters are illustrated in Table I, and the machine works in the motor mode. The torque transducer is set up for torque measurement. The magnetic powder brake is used for transferring the torque with the load connected.

Figure 12 illustrates the implementation flowchart of proposed method. It contains three steps, i.e., calculate the spatial distribution of magductance modulator, calculate the modulated MMF, and calculate the machine performance. Their detailed descriptions are as follows.

Step 1: Calculate the spatial distribution of magductance modulator. According to the specifically machine geometric parameters, calculate the spatial distribution of magductance modulator $\mathcal{L}(\phi)$ from the investigation above.

The geometric parameters of rotor side in the investigated SCIM is shown in Table V. According to (10), the calculated resistance of rotor bar R_b is 0.0561 mΩ. The original resistance of common end ring R_e is 0.001 mΩ. Derived from (5), the equivalent resistance of common end ring R'_e is 0.018 mΩ.

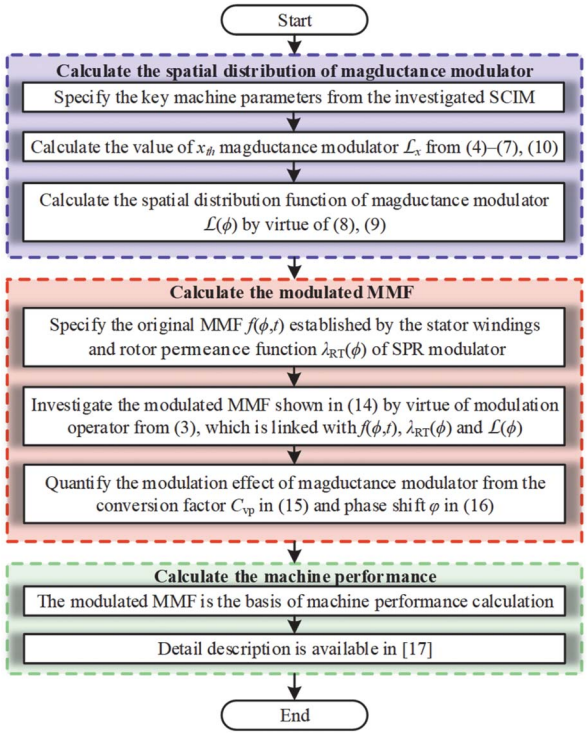

Fig. 12. Implementation flowchart of the proposed method.

TABLE V
Geometric Parameters of Rotor Side

Segment	Variable	Value
Bar	B_{s0}	1 mm
	B_{s1}	5.5 mm
	B_{s2}	3 mm
	H_{s0}	0.5 mm
	H_{s1}	1.3 mm
	H_{s2}	21.7 mm
End ring	End ring width	13.5 mm
	End ring height	31 mm

According to (6) and (7), the value of single magductance modulator $\mathcal{L}_2$ is 1975.63 Ω^{-1} when $N_{SC} = 26$. On the basis of description above, plot the spatial distribution of magductance modulator, and the result is illustrated in Fig. 6.

Step 2: Calculate the modulated MMF. Derived from the modulation operator, additionally $\mathcal{L}(\phi)$, it is essential to determine $\lambda_{RT}(\phi)$ and $f(\phi, t)$ respectively according to (11) and (12). For (12), the current amplitude of stator windings I_m is illustrated in Fig. 13. Then combined with $\mathcal{L}(\phi)$, the modulated MMF is calculated, and the magnetic field conversion factor C_{vp} and phase shift φ are available.

According to the investigated machine whose parameters are illustrated in Table I, from (15) and (16), the calculated magnetic field conversion factor C_{vp} and phase shift φ versus slip frequency s are illustrated in Fig. 14. It can be seen that, with an increase in s, the modulation effect of magductance

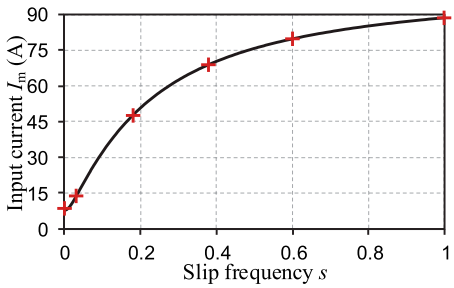

Fig. 13. Current amplitude of stator windings I_m.

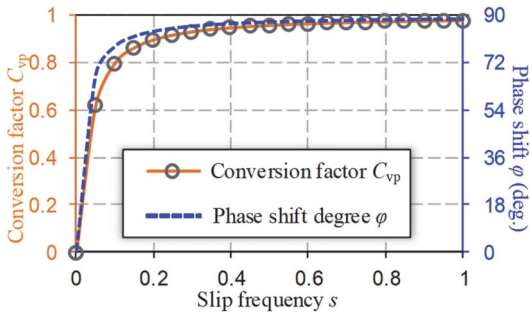

Fig. 14. C_{vp} and φ versus slip frequency s.

modulator increases and φ also keeps increasing. When s approaches 1, φ is close to 90° and C_{vp} is close to 1. At this time, it can be considered that most of MMF are modulated by the magductance modulator. When the modulated MMF is available, the machine performance can be calculated.

Step 3: Calculate the machine performance. Derived from *Step 2*, when the modulated MMF is available, the machine performance can be investigated from the description in [17].

The expression for average torque T_{avg} can be expressed as

$$T_{avg} = \frac{1}{T}\int_0^T \left\{ \frac{\mu_0 r_g^2 l_{stk}}{2g} \frac{\partial}{\partial \Delta} \int_0^{2\pi} M(\mathcal{L})[f(\phi,t)]^2 d\phi \right\} dt = \frac{p\mu_0 \pi r_g l_{stk}}{g} F_1^2 C_{vp} \cos(\varphi) \quad (17)$$

where r_g is the airgap radius.

According to *Step 2*, with an increase in s, C_{vp}, and φ increase. From (17), C_{vp} and φ are linked with the value of T_{avg}. T_{avg} is proportional to C_{vp} and unproportional to φ which is denoted by $\cos(\varphi)$. Contrary influences of them two on machine performance mean that there exists a critical slip frequency, which corresponds to the maximum torque. The calculated results are compared with the FEA and experimental ones as illustrated in Fig. 15, with various torque results illustrated in Table VI. To investigate the end effects more effectively, the 3-D FEA is also applied as illustrated in Fig. 16. Besides, the torque results from the classical equivalent electrical circuit method [1], [2], [3] are also calculated to be compared with that from the proposed method.

The variation trend of average torque versus s is in accordance with the theoretical analysis above. When s is small, torque results from various methods are able to coincide well with each other. With an increase in s, the effect of magnetic saturation and magnetic flux leakage, etc., on machine performance

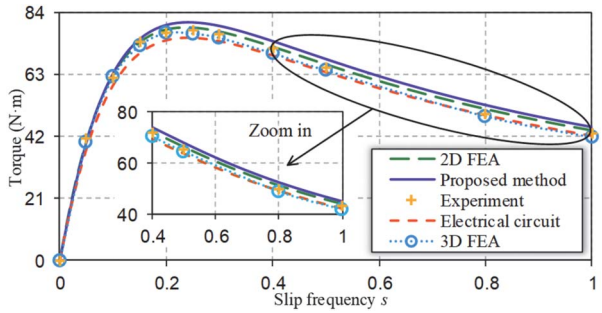

Fig. 15. Torque characteristic of the SCIM calculated from various methods to be compared.

TABLE VI
COMPARISONS OF TORQUE RESULTS

s	2-D FEA (N·m)	3-D FEA (N·m)	Electrical Circuit (N·m)	Proposed Method (N·m)	Experiments (N·m)
0.1	62.7	62.1	59.4	63.2	61.8
0.2	77.9	77	74.7	79.6	77
0.3	77.2	75.4	74.3	79.2	76.6
0.5	66.2	64.4	64	68	65.2
0.8	51.1	48.8	49.3	52.5	49

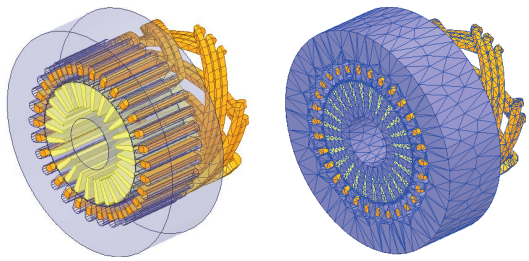

(a) (b)

Fig. 16. 3-D FEA model of the investigated SCIM. (a) Machine topology. (b) Mesh plot.

also increases correspondingly. Therefore, the calculated torque results from proposed method are larger than those from other results. Different from 3-D FEA that directly investigates the end effects during the calculation process, the 2-D FEA considers the end effects from rotor end rings through introducing the end ring impedances as lumped parameters into the calculation process. It is available that the torque results from 2-D FEA are larger than that from 3-D FEA. There is a better fit between results from 3-D FEA and experimental measurements, compared with that from 2-D FEA and experimental ones. It reveals that the differences in end effects between 2-D FEA and 3-D FEA inevitably have effects on SCIM performance. All of these results are within the reasonable error range however.

A comparison of torque results from the electrical circuit method and proposed method also reveals the effectiveness of proposed method in analytical calculation. Similarly, the torque results from winding function method [4], [5], [6] can also be calculated to validate the proposed method. There is no doubt that both the electrical circuit method and winding function method are capable of calculating the machine performance accurately. Compared with them, the proposed method allows for a chance of calculating the machine performance directly in

magnetic field parameters, understanding the SCIM working principle from a new perspective, and conducting the analysis of SCC modulator as similar as that of SPR and FBS modulator.

Besides, it should be noted that, not only the amplitude modulation which is reflected by C_{vp} but also the phase modulation from φ should be considered in the calculation process of SCIM machine performance.

V. Conclusion

This article introduced the magductance modulator into the SCIM. The calculation method for magductance of the squirrel cage was presented, taking the end effects into consideration. Its modulation operator was expressed directly in magnetic field parameters, i.e., reluctance and magductance. Unique vector modulation was effectively illustrated, enabling the proposed method to accurately evaluate machine performance and investigate the phase modulation effect. It was found that the magnetic field conversion factor C_{vp} and phase shift φ are closely associated with machine performance. Furthermore, the proposed method allowed for a comprehensive investigation of the effects of modulator parameters, including the number of rotor bars, material usage, and radial length. The analytical results obtained from the proposed method coincided well with FEA ones. Thus, introducing the concept of magductance modulator facilitated the analysis and optimization of modulator parameters in a manner similar to the SPR modulator and FBS modulator. The proposed method can be extended to other SCIMs. While it should also be noted that the proposed method in this article focused on the normal operation of SCIM, and the situation of rotor bar faults or end ring faults were not considered. In addition to the SCIM, when considering the complex magnetic field modulation behavior in the brushless doubly-fed IM, the chance of introducing the magductance into the analysis of brushless doubly-fed IM deserves to be further investigated.

References

[1] C. G. Veinott, "Performance calculations on induction motors practical straightforward means for calculating performance of single-phase or polyphase induction motors," *Trans. Am. Inst. Electr. Eng.*, vol. 51, no. 3, pp. 743–754, Sep. 1932.

[2] P. D. Agarwal, "Equivalent circuits and performance calculations of canned motors," *Trans. Am. Inst. Electr. Eng.*, vol. 79, no. 3, pp. 635–642, Apr. 1960.

[3] Z. Yang, Q. Ding, X. Sun, and C. Lu, "Design and analysis of a three-speed wound bearingless induction motor," *IEEE Trans. Ind. Electron.*, vol. 69, no. 12, pp. 12529–12539, Dec. 2022.

[4] H. A. Toliyat, T. A. Lipo, and J. C. White, "Analysis of a concentrated winding induction machine for adjustable speed drive applications. I. Motor analysis," *IEEE Trans. Energy Convers.*, vol. 6, no. 4, pp. 679–683, Dec. 1991.

[5] J. Marault, A. Tounzi, F. Gillon, and M. Hecquet, "Efficient approach based on equivalent electric circuit model to determine rotor bar currents of squirrel cage induction machines," *IEEE Trans. Magn.*, vol. 57, no. 2, Feb. 2021, Art. no. 8101305.

[6] J. Liu, C. Di, and X. Bao, "An efficient air-gap flux density analysis method for the design of induction machines," *IEEE Trans. Magn.*, vol. 58, no. 8, Aug. 2022. Art. no. 8106406.

[7] M. Cheng, P. Han, and W. Hua, "General airgap field modulation theory for electrical machines," *IEEE Trans. Ind. Electron.*, vol. 64, no. 8, pp. 6063–6074, Aug. 2017.

[8] M. Cheng, P. Han, Y. Du, and H. Wen, *General Airgap Field Modulation Theory for Electrical Machines: Principles and Practice.* Hoboken, NJ, USA: Wiley, Jan. 2023.

[9] M. Cheng, H. Wen, and P. Han, "Analysis of airgap field modulation principle of simple salient poles," *IEEE Trans. Ind. Electron.*, vol. 66, no. 4, pp. 2628–2638, Apr. 2019.

[10] P. Han, J. Zhang, and M. Cheng, "Analytical analysis and performance characterization of brushless doubly fed machines with multibarrier rotors," *IEEE Trans. Ind. Appl.*, vol. 55, no. 6, pp. 5758–5767, Nov./Dec. 2019.

[11] Z. Ma, M. Cheng, and H. Wen, "Analysis and optimization of rotor salient pole reluctance considering multi–modulation orders," *IEEE Trans. Ind. Electron.*, vol. 70, no. 11, pp. 10871–10880, Nov. 2023.

[12] H. Wen and M. Cheng, "Unified analysis of induction machine and synchronous machine based on the general airgap field modulation theory," *IEEE Trans. Ind. Electron.*, vol. 66, no. 12, pp. 9205–9216, Dec. 2019.

[13] M. D. Nardo, A. Marfoli, M. Degano, and C. Gerada, "Rotor slot design of squirrel cage induction motors with improved rated efficiency and starting capability," *IEEE Trans. Ind. Appl.*, vol. 58, no. 3, pp. 3383–3393, May/Jun. 2022.

[14] X. Wang, T. D. Strous, D. Lahaye, H. Polinder, and J. A. Ferreira, "Modeling and optimization of brushless doubly-fed induction machines using computationally efficient finite-element analysis," *IEEE Trans. Ind. Appl.*, vol. 52, no. 6, pp. 4525–4534, Nov./Dec. 2016.

[15] P. Han, P. Peng, W. Qin, and M. Cheng, "Theoretical and experimental reevaluation of short-circuited rotor windings in induction machines," in *Proc. IEEE Energy Convers. Congr. Expo*, Detroit, MI, USA, Oct. 2022, pp. 01–06.

[16] M. Cheng, W. Qin, X. Zhu, and Z. Wang, "Magnetic-inductance: Concept, definition, and applications," *IEEE Trans. Power Electron.*, vol. 37, no. 10, pp. 12406–12414, Oct. 2022.

[17] M. Cheng, P. Han, Y. Du, H. Wen, and X. Li, "A tutorial on general air-gap field modulation theory for electrical machines," *IEEE J. Emerg. Sel. Top. Power Electron.*, vol. 10, no. 2, pp. 1712–1732, Apr. 2022.

[18] A. Marfoli, L. Papini, P. Bolognesi, and C. Gerada, "An analytical-numerical approach to model and analyse squirrel cage induction motors," *IEEE Trans. Energy Convers.*, vol. 36, no. 1, pp. 421–430, Mar. 2021.

[19] X. Wang, C. Zhu, R. Zhang, R. Tang, and H. Song-Yop, "Performance analysis of single-phase induction motor based on voltage source complex finite-element analysis," *IEEE Trans. Magn.*, vol. 42, no. 4, pp. 587–590, Apr. 2006.

[20] K. Yamazaki, "An efficient procedure to calculate equivalent circuit parameter of induction motor using 3-D nonlinear time-stepping finite-element method," *IEEE Trans. Magn.*, vol. 38, no. 2, pp. 1281–1284, Mar. 2002.

[21] D. G. Dorrell, "Calculation and effects of end-ring impedance in cage induction motors," *IEEE Trans. Magn.*, vol. 41, no. 3, pp. 1176–1183, Mar. 2005.

[22] P. Lombard and F. Zidat, "Determining end ring resistance and inductance of squirrel cage for induction motor with 2D and 3D computations," in *Proc. Int. Conf. Elect. Mach. (ICEM)*, Lausanne, Switzerland, 2016, pp. 266–271.

[23] J. Yu, C. Liu, Z. Song, and H. Zhao, "Permeance and inductance modeling of a double-stator hybrid-excited flux-switching permanent-magnet machine," *IEEE Trans. Transp. Electrific.*, vol. 6, no. 3, pp. 1134–1145, Sep. 2020.

[24] Q. Chen, Y. Yan, G. Xu, M. Xu, and G. Liu, "Principle of torque ripple reduction in synchronous reluctance motors with shifted asymmetrical poles," *IEEE J. Emerg. Sel. Top. Power Electron.*, vol. 8, no. 3, pp. 2611–2622, Sep. 2020.

[25] X. Chen, W. Pan, and X. Wang, "Analytical calculation of air-gap magnetic field in brushless doubly-fed reluctance machine with flux barriers," *IEEE Trans. Energy Convers.*, vol. 37, no. 2, pp. 1292–1303, Jun. 2022.

Zhengzhou Ma (Student Member, IEEE) was born in Yancheng, China, in 1999. He received the B.Sc. degree in electrical engineering from Hohai University, Nanjing, China, in 2021. He is currently working towards the Ph.D. degree in electrical engineering with the School of Electrical Engineering, Southeast University, Nanjing.

His current research interests include the design, analysis and optimization of electrical machines from the view of magnetic field modulation theory.

Ming Cheng (Fellow, IEEE) received the B.Sc. and M.Sc. degrees from Southeast University, Nanjing, China, in 1982 and 1987, respectively, and the Ph.D. degree from the Department of Electrical and Electronic Engineering, The University of Hong Kong, Hong Kong, in 2001, all in electrical engineering.

Since 1987, he has been with Southeast University, where he is currently a Chief Professor with the School of Electrical Engineering and the Director of the Research Center for Wind Power Generation. From 2011, he was a Visiting Professor with the Wisconsin Electric Machine and Power Electronics Consortium, University of Wisconsin, Madison, WI, USA. His teaching and research interests include electrical machines, motor drives for EV, renewable energy generation, and servo motor and control. He has authored or co-authored more than 500 technical papers and 7 books and is the holder of 150 patents in these areas.

Prof. Cheng is a Fellow of the Institution of Engineering and Technology. He has served as the Chair and an Organizing Committee Member for many international conferences. He is a Distinguished Lecturer of the IEEE Industry Application Society in 2015/2016.

Wei Qin (Member, IEEE) received the B.Sc. degree in electrical engineering from Henan Polytechnic University, Jiaozuo, China, in 2016, the M.Sc. degree in power electronics and electrical drives from Nanjing University of Science and Technology, Nanjing, China, in 2019, and the Ph.D. degree in electrical engineering from Southeast University, Nanjing, in 2024.

Since 2024, he has been a Postdoctoral Fellowship with the School of Electrical Engineering, Southeast University. His research interests include magnetic circuit theory and magnetic field modulation theory of electrical machines.

Peng Han received the B.Sc. and Ph.D. degrees in electrical engineering from the School of Electrical Engineering, Southeast University, Nanjing, China, in 2012 and 2017, respectively.

From 2014 to 2015, he was a joint Ph.D. student funded by the China Scholarship Council with the Department of Energy Technology, Aalborg University, Aalborg, Denmark, where he focused on the brushless doubly fed machines for wind energy conversion and high-power drive. He is currently a Postdoctoral Researcher with the SPARK Laboratory, Department of Electrical and Computer Engineering, University of Kentucky, Lexington, KY, USA. His current research interests include electrical machines, power electronics, and renewable energy.

Zheng Wang received the B.Eng. and M.Eng. degrees from Southeast University, Nanjing, China, in 2000 and 2003, respectively, and the Ph.D. degree from the University of Hong Kong, Hong Kong, in 2008, all in electrical engineering.

From 2008 to 2009, he was a Postdoctoral Fellow with Ryerson University, Toronto, ON, Canada. He is currently a Full Professor with the School of Electrical Engineering, Southeast University, Nanjing China. He has authored more than 120 internationally refereed papers, one English book by IEEE-Wiley Press, and two English book chapters on the topics of his research interests, which include electric drives, power electronics, and distributed generation.

Prof. Wang was the recipient of the IEEE PES Chapter Outstanding Engineer Award, First-class Science and Technology Award of Jiangsu Province in China, and Outstanding Young Scholar Award of Jiangsu Natural Science Foundation of China. He is an IET Fellow and an Associate Editor for the IEEE TRANSACTIONS ON INDUSTRIAL ELECTRONICS.

Wei Hua (Senior Member, IEEE) received the B.Sc. and Ph.D. degrees in electrical engineering from Southeast University, Nanjing, China, in 2001 and 2007, respectively.

From 2004 to 2005, he was with the Department of Electronics and Electrical Engineering, The University of Sheffield, U.K., as a Joint-Supervised Ph.D. Student. Since 2007, he has been with the Southeast University, where he is currently a Chief Professor of Southeast University and a Distinguished Professor of Jiangsu Province. From 2010, he has also worked with Yancheng Institute of New Energy Vehicles of Southeast University. He has co-authored over 150 technical papers. He holds 50 patents in his areas of interest. His teaching and research interests include design, analysis, and control of electrical machines, especially for PM brushless machines and switching reluctance machines.